frontiers | Frontiers in Physics

TYPE Original Research
PUBLISHED 18 June 2025
DOI 10.3389/fphy.2025.1595785

OPEN ACCESS

EDITED BY
Rajib Biswas,
Tezpur University, India

REVIEWED BY
Muhammad Ijaz,
Manchester Metropolitan University, United Kingdom
Xiao Sun,
Curtin University, Australia

*CORRESPONDENCE
Imran Aziz,
imran.aziz@physics.uu.se
Ahmad Almogren,
ahalmogren@ksu.edu.sa

RECEIVED 18 March 2025
ACCEPTED 26 May 2025
PUBLISHED 18 June 2025

CITATION
Mirza J, Atieh A, Kanwal B, Kanwal F, Aziz I and Almogren A (2025) Fermentation endpoint detection of Soybean using specially designed *Pd*-coated FBG stress sensor.
Front. Phys. 13:1595785.
doi: 10.3389/fphy.2025.1595785

Fermentation endpoint detection of Soybean using specially designed *Pd*-coated FBG stress sensor

Jawad Mirza[1,2], Ahmad Atieh[3], Benish Kanwal[4], Firdos Kanwal[4], Imran Aziz[4,5]* and Ahmad Almogren[6]*

[1]Electrical Engineering Department, HITEC University Taxila, Taxila, Pakistan, [2]SEECS Photonics Research Group, Islamabad, Pakistan, [3]Optiwave Systems Inc., Ottawa, ON, Canada, [4]Electrical Engineering Department, Mirpur University of Science and Technology (MUST), Mirpur, Pakistan, [5]Department of Physics and Astronomy, Uppsala University, Uppsala, Sweden, [6]Department of Computer Science, College of Computer and Information Sciences, King Saud University, Riyadh, Saudi Arabia

Determining the fermentation endpoint of organic compounds is critical for optimizing yield, ensuring the product consistency, and minimizing byproducts. However, conventional detection methods are slow, labor-intensive, and lack real-time monitoring, limiting their suitability for industrial automation. We propose a novel, non-destructive method for real-time detection of fermentation endpoint of Soybean using Palladium (*Pd*)-coated fiber Bragg grating (FBG) stress sensor. The fermentation endpoint can be detected by monitoring the shift in Bragg wavelength caused by the stress in *Pd*-coated FBG sensor due to the volume expansion of the *Pd* coating upon the formation of Palladium Hydride (PdH_x) after Hydrogen (H_2) gas absorption, which is released as a byproduct during Soybean fermentation. The *Pd*-coated FBG stress sensor is analytically designed and validated using OptiSystem simulation tool, achieving a high sensitivity of 61.6 p.m./MPa. Our findings confirm that this method provides a simple, efficient, and real-time solution for monitoring the fermentation process of organic compounds that produce H_2 offering significant advantages over traditional techniques.

KEYWORDS

fermentation endpoint, Soybean, Palladium, Hydrogen sensing, fiber Bragg grating, wavelength sensitivity, induced stress

1 Introduction

Fermentation of organic compounds is a vital biochemical process with significant applications in food industry, biofuel generation, and biotechnology [1]. It involves the microbial metabolism of organic substrates such as carbohydrates into simpler compounds like alcohols, organic acids, and gases facilitated by bacteria, yeast, and fungi [1]. Detecting the fermentation endpoint is essential to ensure optimal yield, quality, and process efficiency [1]. For example, in the fermentation of Soybean into acetic acid, the process occurs in two stages [1, 2]: the first is the hydrolysis of Soybean proteins and carbohydrates into simpler sugars and amino acids, followed by the oxidation of ethanol to acetic acid by acetic acid bacteria (AAB) such as

acetobacter species. Accurate endpoint detection is crucial to prevent over-oxidation which could degrade acetic acid into carbon dioxide and water, compromising both quality and yield [2]. Advanced analytical techniques, including pH monitoring, gas chromatography, and high-performance liquid chromatography are commonly used to determine the fermentation endpoint and maintain the desired acetic acid concentration. Research emphasizes the importance of controlling factors like temperature, oxygen levels, and microbial activity to optimize the process [2, 3]. Beyond enhancing the nutritional profile of Soy-based products, Soybean fermentation for acetic acid production also yields valuable ingredients for the food industry such as vinegar and condiments, showcasing the broader economic and nutritional significance of fermentation [2, 3].

From an economic perspective, the production of acetic acid from Soybean's fermentation is highly valuable due to its applications in food, pharmaceuticals, and chemicals. This process is cost-effective compared to synthetic production as it utilizes natural source, thus reducing the energy consumption and production costs. The growing demand of acetic acid produced through natural sources has further boosted its market value. The global acetic acid market, valued at over $10 billion in 2022, is projected to grow, driven by its use in food processing, textiles, and biodegradable plastics [4]. Fermentation supports sustainability and creates economic opportunities for agricultural communities by utilizing local raw materials.

2 Related works

Determining the fermentation endpoint in Soybean processing is crucial for ensuring the product quality, maximizing yield, and avoiding over-fermentation which can result in unwanted byproducts. A range of traditional analytical techniques are utilized to identify when fermentation is complete. These methods include pH monitoring [5], gas chromatography (GC) [6], high-performance liquid chromatography (HPLC) [7], and Fourier transform infrared (FTIR) spectroscopy [8]. Analytical methods for fermentation endpoint detection often suffer from limitations such as time consuming sample preparation, high operational costs, potential contamination risks, and need for specialized equipment and expertise. Non-destructive, real-time, and online techniques for fermentation endpoint detection are essential to overcome the limitations of traditional analytical methods ensuring continuous monitoring and improved process efficiency. Various real-time techniques have been proposed to monitor the fermentation endpoint in different organic compounds. For example, monitoring the fermentation in dairy products using fluorescence spectroscopy [5], ultrasonic sensor [9], infrared light backscatter sensor [10], near-infrared (NIR) spectroscopy [11], monitoring the fermentation process in ethanol using viable cell sensor [12], monitoring the fermentation in yeast using software controlled automatic real-time biosensor [13], monitoring the fermentation process in Soybean using miniature fiber NIR spectrometer [14], monitoring the fermentation process in wine with benchtop 1H NMR spectroscopy [15] and NIR spectroscopy [16], and monitoring the fermentation process in black tea using an electronic tongue [17]. The literature review has been further elaborated in Table 1 by comparing the important achievements of past studies with proposed work.

We introduce a novel non-destructive approach for real-time detection of the Soybean fermentation endpoint using a *Pd*-coated FBG stress sensor. This method detects fermentation completion by tracking the Bragg wavelength shift caused by stress in the *Pd*-coated FBG sensor due to *Pd* coating expansion upon PdH_x formation after H_2 absorption which is a key fermentation byproduct. The sensor is analytically designed and validated using OptiSystem simulation tool having a wavelength sensitivity of 61.6 p.m./MPa. This pioneering work establishes a new pathway for real-time monitoring of fermentation processes involving H_2 production.

3 Modelling the fermentation process and working principle

To accurately model the fermentation process of Soybean and explain the working principle of the proposed method, it is important to estimate the total yield of H_2 released as byproduct during fermentation process and the amount of stress induced on the *Pd*-coated FBG sensor by volume expansion of the *Pd* coating due to the formation of PdH_x after absorption of H_2, where x is the ratio of Hydrogen to Palladium. The fermentation of Soybean involves microbial activity that degrades organic compounds, resulting in the production of H_2 alongside other byproducts such as organic acids and carbon dioxide CO_2. The fermentation process of soybean can be expressed by following chemical equation [18].

$$C_6H_{12}O_6 + 2H_2O \rightarrow 2CH_3COOH + 2CO_2 + 4H_2 \quad (1)$$

The Equation 1 illustrates the fermentation process of Glucose ($C_6H_{12}O_6$) which is considered as a primary component in Soybean, into acetic acid (CH_3COOH), CO_2, and H_2. From this equation, it is evident that 1 mol of $C_6H_{12}O_6$ produces 4 mol of H_2. Therefore, the total mass of H_2 produced per kg of $C_6H_{12}O_6$ can be calculated by following steps.

$$\begin{aligned} &\text{Molecular weight of } C_6H_{12}O_6 &&= 80\ \text{g/mol} \\ &\text{Molecular weight of } H_2 &&= 2\ \text{g/mol} \\ &\text{Mass of } 4H_2 &&= 4 \times 2 = 8\ \text{g} \end{aligned}$$

Thus, 180 g of $C_6H_{12}O_6$(1 mol) yields 8 g of H_2. The mass of H_2 produced per kg of $C_6H_{12}O_6$ is calculated as.

$$\frac{8\,\text{g}}{180\,\text{g}} \times 1000 = 44.49\,\text{g}$$

Therefore, 1 kg of $C_6H_{12}O_6$ produces approximately 44.49 g of H_2. As we have considered 5 kg Soybean in this research, therefore 222.5 g (≈2.5 m^3) of H_2 gas is produced as byproduct during the fermentation process. To calculate the volume of H_2 generated during fermentation at STP, we use the ideal gas law. At STP, the molar volume of an ideal gas is 22 L/mol. The molar mass of H_2 is 2 g/mol, so for 222.5 g of H_2, the number of moles is calculated as:

$$\text{Number of moles} = \frac{\text{Mass}}{\text{Molar mass}} = \frac{222.5\ \text{g}}{2\ \text{g/mol}} = 111.25\,\text{mol}.$$

TABLE 1 Elaboration of the literature survey and comparison with proposed work.

Study	Organic compound	Technique	Sensing type
[5]	Yogurt	Offline and destructive	pH monitoring
[6]	Milk	Offline and destructive	Gas chromatography
[7]	Grapes	Offline and destructive	Liquid chromatography
[8]	Oat and pea	Offline and destructive	FTIR spectroscopy
[9]	Yogurt	Online and non-destructive	Ultrasonic measurement
[10]	Milk	Online and non-destructive	Light scattering
[11]	Yogurt	Online and non-destructive	NIR spectroscopy
[12]	Ethanol	Online and non-destructive	Cell sensor
[13]	Yeast	Online and non-destructive	Biosensor
[14]	Soybean	Online and non-destructive	NIR spectroscopy
[15]	Wine	Online and non-destructive	1H NMR spectroscopy
[16]	Wine	Online and non-destructive	NIR spectroscopy
[17]	Black tea	Online and non-destructive	Electronic tongue
Proposed	Soybean	Online and non-destructive	FBG sensing

Using the molar volume of an ideal gas at STP, the volume of H_2 gas is:

$$\begin{aligned}\text{Volume} &= \text{Number of moles} \\ &\times \text{Molar volume} \\ &= 111.25\,\text{mol} \times 22.4\,\text{L/mol} \\ &= 2492\,\text{L}.\end{aligned}$$

Converting liters to cubic meters (since $1\,\text{m}^3 = 1000\,\text{L}$), the volume of H_2 generated at STP is:

$$\text{Volume} = \frac{2492\,\text{L}}{1000} = 2.492\,\text{m}^3.$$

To determine the stress induced in *Pd*-coated FBG sensor when exposed to 222.5 g of H_2, first we need to consider the H_2 absorption in *Pd* coating, saturation limit of PdH_x formation, and stress-strain relationship. Then we shall be able to calculate the shift in Bragg wavelength of FBG stress sensor.

3.1 H_2 absorption capacity of *Pd* and saturation limit of PdH_x

Figure 1 illustrates the fabrication of *Pd*-coated FBG sensors which involves three critical steps. First, the FBG is inscribed in the core of single-mode fiber (SMF) using a UV laser as shown in Figure 1a to create the periodic refractive index variation. Second, the fiber cladding is selectively etched using hydrofluoric acid to reduce the diameter exposing the core as shown in Figure 1b.

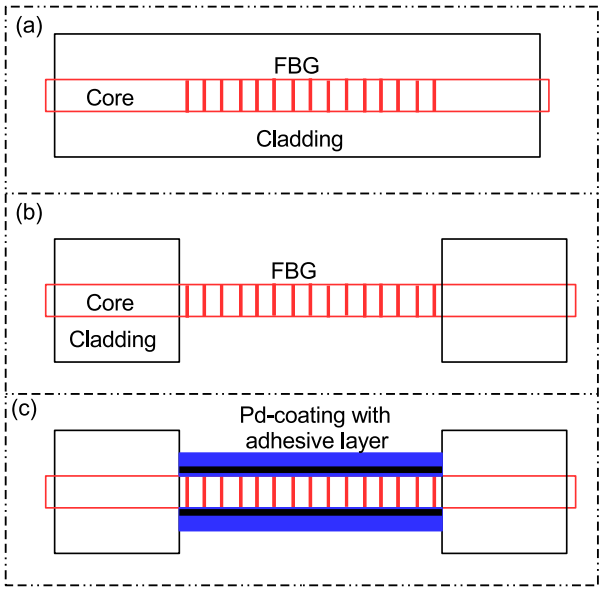

FIGURE 1
Important steps for *Pd* coating on FBG **(a)** FBG without etched cladding **(b)** FBG with etched cladding **(c)** Deposition of *Pd* coating alongwith adhesive layer.

Finally, a uniform *Pd* layer of 50–200 nm thickness is deposited either through sputtering or electroless plating as illustrated in Figure 1c.

TABLE 2 Comparison of parameters for the analytical model and OptiSystem analysis of the *Pd*-coated FBG stress sensor.

Sr. No	Parameters	Numerical model	OptiSystem model
1	Initial Bragg wavelength	1,550 nm	1,550 nm
2	Core radius	4.6 μm	4.6 μm
3	Cladding radius	62.5 μm	62.5 μm
4	Thickness of *Pd* layer	100 nm	100 nm
5	Young's modulus of *Pd*	1,200 MPa	1,200 MPa
6	Poisson's ratio of *Pd*	0.39	0.2
7	Photoelastic constant of the Silica fiber	0.22	0.9

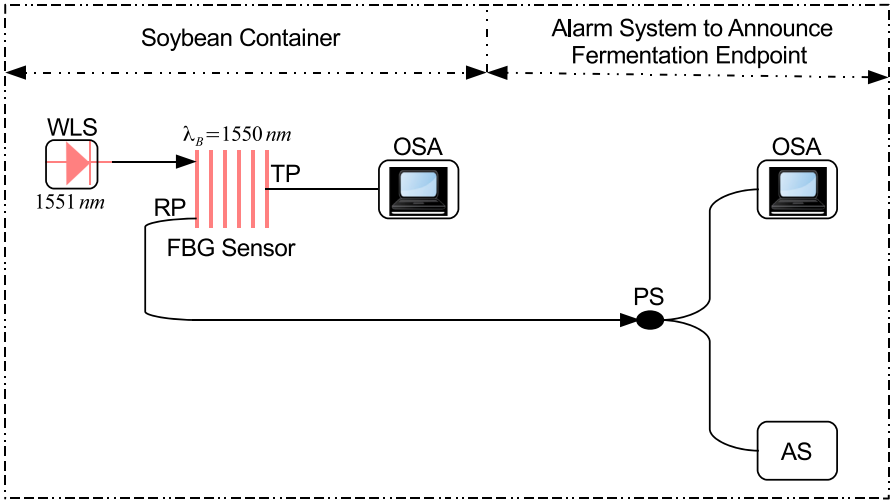

FIGURE 2
Block diagram of the sensor setup designed in Optisystem. WLS: White light source, FBG: Fiber Bragg grating stress sensor, PS: Power splitter, OSA: Optical spectrum analyzer, AS: Alam system.

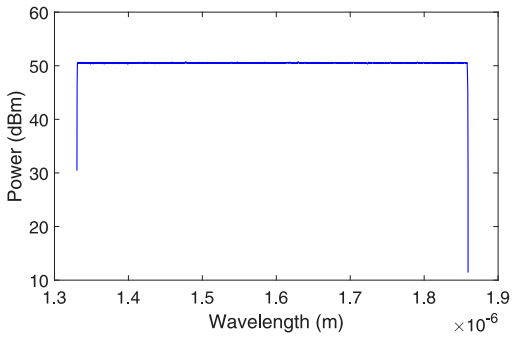

FIGURE 3
Spectral plot of WLS centered at 1551 nm.

First of all, the reaction between *Pd* and H_2 to form PdH_x is represented by Equation 2 which is reversible equilibrium Equation 19.

$$\mathrm{Pd} + \frac{x}{2}\mathrm{H_2} \leftrightarrow \mathrm{PdH}_x \tag{2}$$

The absorption of H_2 in *Pd* occurs up to a maximum atomic ratio of $\frac{\mathrm{H}}{\mathrm{Pd}} = x = 0.65$ which represents the maximum saturation limit. This implies that while the total available amount of H_2 may be around 222.5 g, *Pd* can only absorbs H_2 up to its saturation. Consequently, stress development in *Pd* layer is confined to the period during which it becomes fully saturated with H_2. Once saturation is achieved, any excess H_2 does not contribute to further stress development. It is also pertinent to mention that H_2 absorption can be controlled to obtain the required value of x either by reducing the H_2 exposure time or using the *Pd* alloy with lower absorption capacity or using a buffer layer to limit the *Pd* expansion.

3.2 Calculation of stress developed in *Pd* coating

To calculate the stress induced in *Pd*-coated FBG sensor, the following assumptions are crucial to consider.

TABLE 3 List of simulation parameters.

Sr. No	Parameters	Values
1	Operating wavelength of WLS	1,551 nm
2	Initial Bragg wavelength of FBG	1,550 nm
3	Power spectral density of WLS	−60 dBm/Hz
4	Effective index of FBG	1.45
5	Grating length	10 mm
6	Resolution bandwidth of OSA	0.1 nm
7	Sequence length	1,024 bits
8	Samples per bit	512

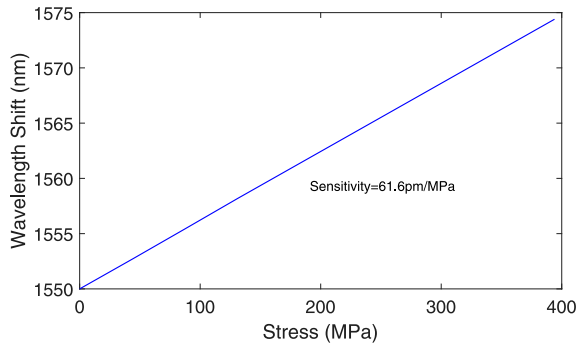

FIGURE 4
Induced stress versus wavelength shift plot.

- Radii of the core and cladding are 4.6 μm and 62.5 μm, respectively.
- Thickness of *Pd* layer over FBG sensor is 100 nm.
- Thickness of adhesive layer of Titanium is 20 nm.
- Saturation limit of 0.1 is considered.
- The effect of temperature on Bragg wavelength shift is not considered in this research.

The strain induced in the *Pd* coating due to H_2 absorption is given by the relation.

$$\varepsilon_{PdH} = 0.2 \times x \tag{3}$$

In Equation 3, x is the atomic ratio of H to *Pd* and 0.2 is the empirical coefficient of expansion. At $x = 0.1$, the value of induced strain is $\varepsilon_{PdH} = 0.2 \times 0.1 = 0.02$. Therefore, the stress in *Pd*-coated FBG sensor due to H_2 absorption is given by the following equation.

$$\sigma PdH = \frac{E_{Pd}}{1 - \nu Pd} \times \varepsilon PdH \tag{4}$$

In Equation 4, σ_{PdH} is the stress induced in *Pd* due to H_2 absorption, $E_{Pd} = 12 \times 10^9$ Pa is the Young's modulus of *Pd*, and $v_{Pd} = 0.39$ is the Poisson's ratio of *Pd*. Therefore, the value of stress at $x = 0.1$ is around 393.44 MPa.

3.3 Effect of stress on Bragg wavelength shift

The shift in the Bragg wavelength (λ_B) of *Pd*-coated FBG sensor due to axial strain after absorbing H_2 is given by the equation [20].

$$\Delta\lambda_B = \lambda_B (1 - P_e) \cdot \varepsilon \tag{5}$$

where P_e is the effective photoelastic constant of the fiber (≈0.22 for silica fibers), ε is the strain in the FBG sensor (≈0.02 at saturation), and λ_B is the initial Bragg wavelength (typically ≈1,550 nm). Applying these values in Equation 5, the shift in Bragg wavelength ($\Delta\lambda_B$) is around 24.2 nm. This is the maximum shift in the Bragg wavelength, which corresponds to a stress of 393.44 MPa induced in FBG sensor when exposed to 222.5 g of H_2 that is released during the fermentation process.

The Bragg wavelength shift of 24.2 nm serves as a key indicator for detecting the fermentation endpoint in Soybean processing. This shift results from the stress-induced expansion of the *Pd* coating on the FBG sensor due to H_2 absorption and the subsequent formation of PdH_x. Since H_2 is a byproduct of soybean fermentation, the observed wavelength shift directly correlates with the completion of the fermentation process.

4 Design validation of *Pd*-coated FBG stress sensor using OptiSystem

The analytical model of the *Pd*-coated FBG stress sensor that is developed in the last section produces a Bragg wavelength shift of 24.2 nm is analyzed using OptiSystem simulation tool. Table 2 compares the parameters used in the analytical model with those employed in OptiSystem for design analysis. Using the parameters of the OptiSystem model, a shift of 24.5 nm in Bragg wavelength is achieved which is comparable to the analytical model making the assumption reasonable.

5 Simulation setup

Figure 2 shows the block diagram of the simulation setup designed in OptiSystem to detect the fermentation endpoint of Soybean. A white light source (WLS) with a power spectral density (PSD) and center wavelength of −60 dBm/Hz and 1,551 nm, respectively is used to illuminate the FBG stress sensor. Figure 3 illustrates the spectrum of WLS. The WLS model used in OptiSystem generates noise bins or sampled signals at the output according to the following mathematical expression.

$$\begin{bmatrix} E_x(t) \\ E_y(t) \end{bmatrix} = \begin{bmatrix} x_x(t) + jy_x(t) \\ x_y(t) + jy_y(t) \end{bmatrix} \cdot \sqrt{\frac{P}{4}} \tag{6}$$

In Equation 6, E is the optical field and P is average power. In the above equation, a Gaussian distribution has been assumed to describe the probability density function (PDF) for the real and imaginary parts of the optical field components E_x and E_y. A broadband light source is essential for FBG sensors because it provides a wide spectral range to accurately track the shifts in

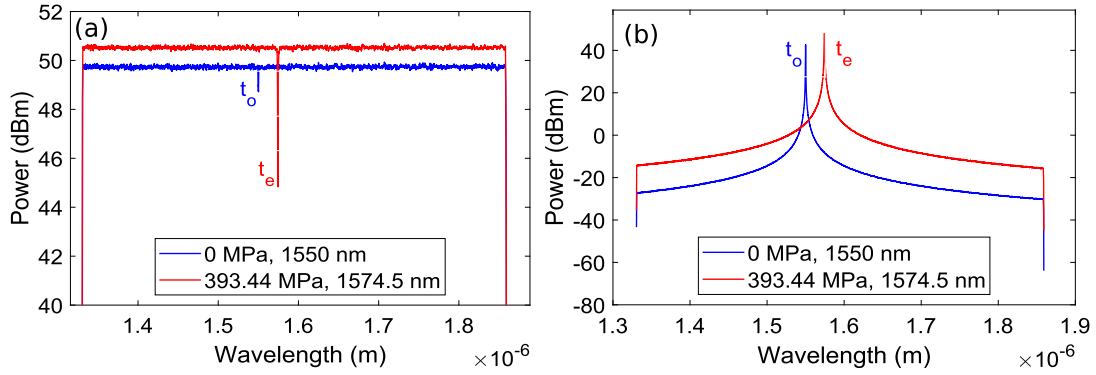

FIGURE 5
(a) Transmission spectra of FBG stress sensor **(b)** Reflection spectra of FBG stress sensor.

Bragg wavelength caused by external perturbations [21]. Unlike narrowband lasers that require fast scanning to avoid missing signal detection, WLS enables high-resolution detection of small wavelength changes which are critical for real-time monitoring in applications like *Pd*-coated FBG stress sensor [21]. Additionally, broadband light sources support multiplexing of multiple FBGs on a single fiber, making it ideal for scalable industrial systems. Its stable and noise-resistant output ensures reliable measurement of stress-induced shifts which are vital for precise fermentation endpoint detection [21]. In practical scenario, the *Pd*-coated FBG stress sensor will be placed inside the fermentation container holding 5 kg of Soybean with a suitable microbial culture to initiate the fermentation process. The temperature, humidity, and pressure inside the container is controlled to ensure optimal fermentation conditions. The *Pd* layer serves as the active sensing material, absorbing H_2 molecules released during fermentation. Upon absorption, *Pd* undergoes a phase transition to PdH_x, leading to volumetric expansion which induces mechanical strain inside the FBG sensor. This strain modifies the grating period of the FBG, causing a Bragg wavelength shift which serves as an indicator of the fermentation endpoint. In OptiSystem, this process is realized using the numerical values of stress calculated in Section 3 to create the corresponding shift in Bragg wavelength of stress sensor. The optical signal reflected from the FBG stress sensor at a shifted Bragg wavelength corresponding to the applied stress, is split into two parts using a 20:80 power splitter (PS) attached to the sensor's reflection port (RP). The 20% output of the PS is sent to an optical spectrum analyzer (OSA) for analysis of the results while the 80% output is connected to the alarm system (AS) for annunciation of the fermentation endpoint. Similarly, the transmitted spectrum is directed to another OSA via the transmission port (TP) for analysis. The important simulation parameters used in this work are described in Table 3.

6 Results and discussion

Figure 4 illustrates the induced stress due to formation of PdH_x after absorbing H_2 by *Pd*-coated FBG sensor versus wavelength shift. It is clear that wavelength sensitivity of 61.6 p.m./MPa has been achieved. A linear relationship between the wavelength shift and induced stress can be observed. The reason of linear relationship between the wavelength shift and the stress shown in Figure 4 is attributed to the fundamental principle of opto-mechanical coupling as expressed in Equation 5. We acknowledge that practical scenarios may introduce noise and nonlinearities due to thermal fluctuations, mechanical vibrations, material hysteresis, and deformations in the *Pd* coating which can affect wavelength shift and resolution. However, the reported sensitivity threshold of 61.6 p.m./MPa sets a floor for the FBG interrogators. Figure 5a shows the transmission spectra of the FBG sensor for stress values of 0 MPa and 393.44 MPa obtained by connecting the OSA to TP of FBG stress sensor as illustrated in Figure 2. Similarly, Figure 5b shows the reflection spectra of FBG the sensor for stress values of 0 MPa and 393.44 MPa indicating the onset and endpoint of fermentation process, respectively. Reflection spectra is obtained by connecting the OSA with 20% output of the PS, that is connected with RP of the FBG stress sensor as shown in Figure 2. Assuming the fermentation starts at time t_o, the transmission dip and the reflection peak of the transmitted and reflected optical signals, respectively equal to the initial Bragg wavelength of *Pd*-coated FBG sensor which is 1,550 nm, as shown in Figure 5 corresponding to the absence of detectable H_2. As fermentation process progresses, microbial activity produces H_2 which is absorbed by the *Pd* coating forming PdH_x. This induces stress in the *Pd*-coated FBG stress sensor, linearly shifting the Bragg wavelength of reflected optical signal. Similarly, the fermentation endpoint is achieved at time t_e. Consequently, the absorption of H_2 in *Pd* coating saturates and any excess H_2 will not contribute to further stress development. The transmission dip and reflection peak of transmitted and reflected optical signals equal to 1,574.5 nm. A maximum shift of 24.5 nm in Bragg wavelength corresponding to a stress of 393.44 MPa is induced in FBG sensor indicating the fermentation endpoint.

7 Conclusion

In this study, we demonstrated a non-destructive and real-time method for detecting the fermentation endpoint of Soybeans using a *Pd*-coated fiber Bragg grating stress sensor. The method

relies on monitoring the shift in the Bragg wavelength, which is caused by the stress induced in the *Pd*-coated FBG sensor due to the volume expansion of the Palladium layer upon the formation of Palladium Hydride after absorbing Hydrogen gas released as a byproduct during the fermentation of Soybeans. The *Pd*-coated fiber Bragg grating sensor was analytically designed and its performance was analyzed using the OptiSystem simulation tool, achieving a wavelength sensitivity of 61.6 p.m./MPa. The results demonstrate that the proposed method provides a reliable, straightforward, and efficient solution for real-time monitoring and detection of the fermentation endpoint of various organic compounds that release Hydrogen gas as a byproduct. This approach holds significant potential for applications in food processing, biotechnology, and industrial fermentation processes.

Data availability statement

The raw data supporting the conclusions of this article will be made available by the authors, without undue reservation.

Author contributions

JM: Conceptualization, Project administration, Software, Validation, Writing – original draft, Writing – review and editing. AA: Methodology, Writing – review and editing. BK: Conceptualization, Investigation, Writing – original draft. FK: Investigation, Methodology, Software, Writing – original draft. IA: Funding acquisition, Resources, Software, Writing – original draft, Writing – review and editing. AA: Resources, Software, Writing – original draft.

Funding

The author(s) declare that financial support was received for the research and/or publication of this article.

Acknowledgments

This work was supported by King Saud University, Riyadh, Saudi Arabia, through ongoing research funding program (ORF-2025-184).

Conflict of interest

Author AA was employed by Optiwave Systems Inc.

The remaining authors declare that the research was conducted in the absence of any commercial or financial relationships that could be construed as a potential conflict of interest.

Generative AI statement

The author(s) declare that no Generative AI was used in the creation of this manuscript.

Publisher's note

All claims expressed in this article are solely those of the authors and do not necessarily represent those of their affiliated organizations, or those of the publisher, the editors and the reviewers. Any product that may be evaluated in this article, or claim that may be made by its manufacturer, is not guaranteed or endorsed by the publisher.

References

1. Wang Y, Wu J, Lv M, Shao Z, Hungwe M, Wang J, et al. Metabolism characteristics of lactic acid bacteria and the expanding applications in food industry. *Front Bioeng Biotechnol* (2021) 9:612285. doi:10.3389/fbioe.2021.612285

2. Zhang Y, Li X, Chen X. Optimization of acetic acid fermentation from soybean meal hydrolysate using response surface methodology. *J Food Sci Technology* (2020) 57(5):1785–94.

3. Wang Y, Li Y, Liu Y. Advances in acetic acid fermentation: mechanisms, challenges, and applications. *Biotechnol Adv* (2019) 37(6):107410.

4. Grand View Research. Acetic acid market size, share and trends analysis report (2022). Available online at: https://www.grandviewresearch.com/industry-analysis/acetic-acid-market (Accessed on February 11, 2025).

5. Mains TP, Payne FA, Sama MP. Monitoring yogurt culture fermentation and predicting fermentation endpoint with fluorescence spectroscopy. *Trans ASABE* (2017) 60(2):529–36.

6. Cui Y, Shi X, Tang Y, Xie Y, Du Z. The effects of heat treatment and fermentation processes on the formation of furfurals in milk-based dairy products using a QuEChERS technique followed by gas chromatography coupled with triple quadrupole mass spectrometry. *Food Chem* (2020) 313:125930. doi:10.1016/j.foodchem.2019.125930

7. Topic Bozic J, Butinar L, Curko N, Kovacevic Ganic K, Mozetic Vodopivec B, Korte D, et al. Implementation of high performance liquid chromatography coupled to thermal lens spectrometry (HPLC-TLS) for quantification of pyranoanthocyanins during fermentation of Pinot Noir grapes. *SN Appl Sci* (2020) 2:1–15.

8. Greulich O, Duedahl-Olesen L, Mikkelsen MS, Smedsgaard J, Bang-Berthelsen CH. Fourier transform infrared spectroscopy tracking of fermentation of oat and pea bases for yoghurt-type products. *Fermentation* (2024) 10(4):189. doi:10.3390/fermentation10040189

9. Bowler A, Ozturk S, di Bari V, Glover ZJ, Watson NJ. Machine learning and domain adaptation to monitor yoghurt fermentation using ultrasonic measurements. *Food Control* (2023) 147:109622. doi:10.1016/j.foodcont.2023.109622

10. Ramezani M, Ferrentino G, Morozova K, Scampicchio M. Multiple light scattering measurements for online monitoring of milk fermentation. *Foods* (2021) 10(7):1582. doi:10.3390/foods10071582

11. Muncan J, Tei K, Tsenkova R. Real-time monitoring of yogurt fermentation process by aquaphotomics near-infrared spectroscopy. *Sensors* (2020) 21(1):177. doi:10.3390/s21010177

12. Feng Y, Tian X, Chen Y, Wang Z, Xia J, Qian J, et al. Real-time and on-line monitoring of ethanol fermentation process by viable cell sensor and electronic nose. *Bioresources and Bioprocessing* (2021) 8(1):37. doi:10.1186/s40643-021-00391-5

13. Lidgren L, Lilja O, Krook M, Kriz D. Automatic fermentation control based on a real-time *in situ* SIRE biosensor regulated glucose feed. *Biosens Bioelectron* (2006) 21(10):2010–3. doi:10.1016/j.bios.2005.09.012

14. Zhang Z, Ding Y, Hu F, Liu Z, Lin X, Fu J, et al. Constructing *in-situ* and real-time monitoring methods during soy sauce production by miniature fiber NIR spectrometers. *Food Chem* (2024) 460:140788. doi:10.1016/j.foodchem.2024.140788

15. Phuong J, Salgado B, Heiß J, Steimers E, Nickolaus P, Keller L, et al. Real-time monitoring of fermentation processes in wine production with benchtop ^{1}H NMR spectroscopy. *Food Res Int* (2025) 203:115741. doi:10.1016/j.foodres.2025.115741

16. Nascimento RJAD, Macedo GRD, Santos ESD, Oliveira JAD. Real-time and *in situ* near-infrared spectroscopy (NIRS) for quantitative monitoring of biomass, glucose, ethanol, and glycerine concentrations in an alcoholic

fermentation. *Braz J Chem Eng* (2017) 34(2):459–68. doi:10.1590/0104-6632.20170342s20150347

17. Ghosh A, Bag AK, Sharma P, Tudu B, Sabhapondit S, Baruah BD, et al. Monitoring the fermentation process and detection of optimum fermentation time of black tea using an electronic tongue. *IEEE Sensors J* (2015) 15(11):6255–62. doi:10.1109/jsen.2015.2455535

18. Thauer RK. Biochemistry of methanogenesis: a tribute to marjory stephenson: 1998 marjory stephenson prize lecture. *Microbiology* (1998) 144(9):2377–406. doi:10.1099/00221287-144-9-2377

19. Ping X, Cao X, Cao C, Lei H, Yang C, Cheng Q, et al. Fiber grating hydrogen sensor: progress, challenge and prospect. *Adv Sensor Res* (2024) 3(2):2300088. doi:10.1002/adsr.202300088

20. Mirza J, Kanwal F, Salaria UA, Ghafoor S, Aziz I, Atieh A, et al. Underwater temperature and pressure monitoring for deep-sea SCUBA divers using optical techniques. *Front Phys* (2024) 12:1417293. doi:10.3389/fphy.2024.1417293

21. Hill KO, Meltz G. Fiber Bragg grating technology fundamentals and overview. *J Lightwave Technol* (1997) 15(8):1263–76. doi:10.1109/50.618320